

XCloud-VIP: Virtual Peak Enables Highly Accelerated NMR Spectroscopy and Faithful Quantitative Measures

Di Guo¹, Zhangren Tu², Yi Guo¹, Yirong Zhou², Jian Wang², Zi Wang², Tianyu Qiu², Min Xiao³, Liubin Feng⁴, Yuqing Huang², Donghai Lin⁴, Yongfu You⁵, Amir Goldbourt⁶, and Xiaobo Qu^{*2}

Abstract: *Background:* Nuclear Magnetic Resonance (NMR) spectroscopy is an important bio-engineering tool to determine the metabolic concentrations, molecule structures and so on. The data acquisition time, however, is very long in multi-dimensional NMR. To accelerate data acquisition, non-uniformly sampling is an effective way but may encounter severe spectral distortions and unfaithful quantitative measures when the acceleration factor is high. *Objective:* To reconstruct high fidelity spectra from highly accelerated NMR and achieve much better quantitative measures. *Methods:* A virtual peak (VIP) approach is proposed to self-learn the prior spectral information, such as the central frequency and peak lineshape, and then feed these information into the reconstruction. The proposed method is further implemented with cloud computing to facilitate online, open, and easy access. *Results:* Results on synthetic and experimental data demonstrate that, compared with the state-of-the-art method, the new approach provides much better reconstruction of low-intensity peaks and significantly improves the quantitative measures, including the regression of peak intensity, the distances between nuclear pairs, and concentrations of metabolics in mixtures. *Conclusion:* Self-learning prior peak information can improve the reconstruction and quantitative measures of spectra. *Significance:* This approach enables highly accelerated NMR and may promote time-consuming applications such as quantitative and time-resolved NMR experiments.

Index Terms—machine learning; nuclear magnetic resonance spectroscopy; fast sampling; Hankel matrix

I. INTRODUCTION

NMR spectroscopy is an important analytical tool in medicine, biology and chemistry. Multidimensional NMR provides fruitful information, such as nuclear atom coupling and molecular structures, but the data acquisition time

increases significantly with spectral resolution and dimensionality [1-3].

Accelerating data acquisition is one of the major developments in modern NMR [4-12]. Without changing the equipment, Non-Uniform Sampling (NUS) allows acquiring fewer data points and spectrum reconstruction with proper signal priors [2, 5-9, 15-17], such as spectrum sparsity in compressed sensing[5-8, 18], the minimal number of peaks in low-rank [19-22] and deep learning [10, 11, 23]. Although these methods are powerful for spectrum reconstructions, they still suffer from spectral distortion under a high acceleration factor.

Why is there distortion? A reconstruction means implicitly restoring lots of peak information, including amplitude, frequency, phase and damping factor. The amplitude determines the intensity of a peak and the latter three factors define the location and lineshape of a peak. Thus, these four factors can be treated as the degree of freedom of a spectrum. Hence, if a reconstruction approach is not designed properly, the degree of freedom may be too high to obtain a good spectrum.

To reduce the spectrum distortion, a possible solution is to reduce the degree of freedom by mining the prior information as much as possible. One fundamental approach is to model the acquired signal, i.e. Free Induction Decay (FID), as a linear superposition of exponential functions[19-22, 24-26]. This model is convenient to incorporate priors since each exponential function corresponds to one spectral peak (We call it a physical peak). However, mining each peak (We call it a Virtual Peak, VIP) from the spectrum is not trivial since the spectrum is a superposition signal.

In this paper, we first get a reference spectrum by reconstructing the undersampled FID, then employ the classic Hankel singular value decomposition (SVD) [21, 27, 28] to extract each VIP, and finally feed this information into a proposed signal reconstruction model.

This work was supported by National Natural Science Foundation of China (61871341, 61971361, 61811530021), National Key R&D Program of China (2017YFC0108703), Health-Education Joint Research Project of Fujian Province (2019-WJ-31), Xiamen University Nanqiang Outstanding Talents Program.

1. Di Guo, Yi Guo are with the School of Computer and Information Engineering, Xiamen University of Technology, Xiamen 361024, China.

2. Zhangren Tu, Yirong Zhou, Jian Wang, Zi Wang, Tianyu Qiu, Yuqing Huang, Xiaobo Qu are with the Department of Electronic Science, Biomedical Intelligent Cloud R&D Center, Fujian Provincial Key Laboratory of Plasma and Magnetic Resonance, Xiamen University, Xiamen 361005, China.

3. Min Xiao are with the School of Opto-Electronic and Communication Engineering, Xiamen University of Technology, Xiamen 361024, China.

4. Liubin Feng, Donghai Lin are with the College of Chemistry and Chemical Engineering, Key Laboratory for Chemical Biology of Fujian Province, High-field NMR Center, Xiamen University, Xiamen 361005, China.

5. Yongfu You is with the China Mobile Group, Xiamen 361005, China.

6. Amir Goldbourt is with the School of Chemistry, Tel Aviv University, Tel Aviv 6997801, Israel.

*Corresponding author: quxiaobo@xmu.edu.cn

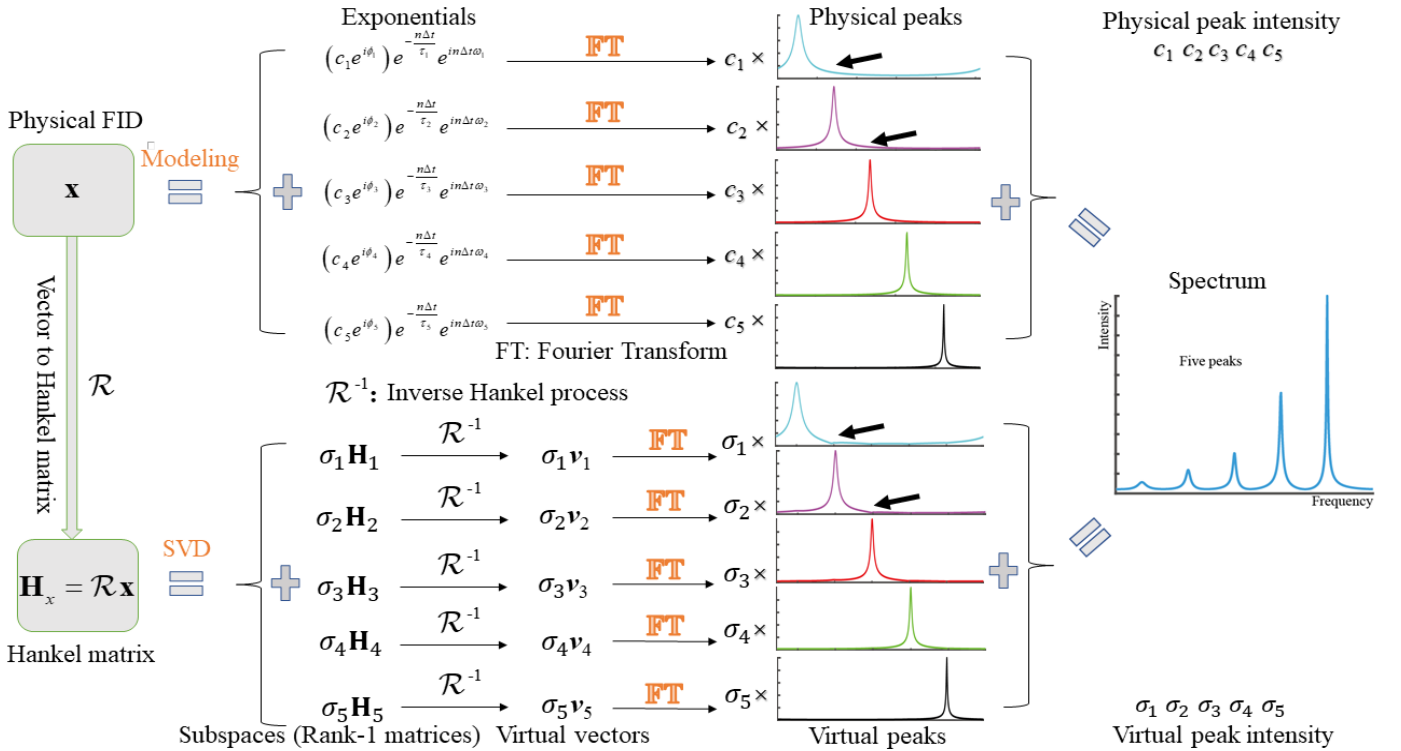


Fig. 1. The schematic of learning virtual peaks (VIPs) from FID. Note: The notation \oplus means the linear combination of these virtual (or physical) peaks will compose the spectrum and the combination weight is called the virtual (or physical) peak intensity.

The structure of the paper as follows: Section II introduces the background. Section III presents a model and derives a numerical algorithm. Section IV describes the experimental result and discussion. Section V gives a conclusion.

II. METHOD

A. Modelling of Virtual Peaks

Our method is based on a basic modelling of FID signal as the sum of exponentials [10, 21, 27, 28] and one property that the number of peaks is equal to the rank of the Hankel matrix converted from the FID [10, 21, 27, 28].

The FID composed of exponentials is modelled as

$$x_n = \sum_{p=1}^P c_p e^{i\phi_p} e^{nM\omega_p} e^{-\frac{n\Delta t}{\tau_p}}, \quad (1)$$

where x_n denotes the n^{th} element of the FID $\mathbf{x} = [x_0, x_1, \dots, x_{2N}]^T$ while c_p , ϕ_p , ω_p and τ_p denote the amplitude, phase, central frequency, damping factor of the p^{th} exponential (or peak), respectively. The total number of exponentials (or peaks) is P . The Δt is the sampling interval and the c_p is the physical peak intensity as shown in Figure 1.

Let \mathcal{R} denote a Hankel operator converting the \mathbf{x} into a Hankel matrix $\mathcal{R}\mathbf{x} \in \mathbb{C}^{N \times N}$, the SVD [10, 21, 27, 28] of $\mathcal{R}\mathbf{x}$ is

$$\mathcal{R}\mathbf{x} = \mathbf{A}\mathbf{\Lambda}\mathbf{B}^H, \quad (2)$$

where \mathbf{A} (or \mathbf{B}) is the left (or right) signal space and $\mathbf{\Lambda}$ is a diagonal matrix called the singular value matrix, the superscript

H denotes the Hermitian transpose. The rank of Hankel matrix is defined as the number of non-zero singular values in $\mathbf{\Lambda}$, whose diagonal entries, i.e. singular values, are commonly stored in the descending order. For a given spectrum with P peaks, the rank of the Hankel matrix is P [21, 28].

The VIP is defined as the spectrum extracted from the rank-1 matrix followed by first averaging all the matrix elements in the anti-diagonal directions and then Fourier transforming. A Hankel matrix with rank P can be linearly combined by a set of rank-1 matrices $\{\mathbf{H}_p \in \mathbb{C}^{N \times N}\}_{p=1,2,\dots,P}$ as

$$\mathcal{R}\mathbf{x} = \sum_{p=1}^P \sigma_p \mathbf{H}_p, \quad (3)$$

where σ_p is the p^{th} singular value stored in $\mathbf{\Lambda}$. For each \mathbf{H}_p , a

inverse Hankel process is defined as \mathcal{R}^{-1} according to

$$\mathcal{R}^{-1}: \mathbb{C}^{N \times N} \rightarrow \mathbb{C}^{2N+1}, \quad (4)$$

by performing the inverse Hankel process using an operator \mathcal{R}^{-1} to convert a subspace matrix \mathbf{H}_p to a vector $\mathbf{x}_p = \mathcal{R}^{-1}\mathbf{H}_p$

via averaging anti-diagonal entries of \mathbf{H}_p . \mathbf{x}_p is also called the virtual vector in Figure 1. Then, a VIP \mathbf{s}_p is obtained by performing the Fourier transform \mathcal{F} on each vector \mathbf{v}_p as

$$\mathbf{s}_p = \mathcal{F}\mathbf{v}_p. \quad (5)$$

Accordingly, the σ_p is the virtual intensity for the p^{th} peak as shown in Figure 1.

The whole process of VIP extraction is shown in Figure 1. This toy example starts with the easily understandable physical peak which is obtained by performing Fourier Transform on each exponential assuming that each function is known.

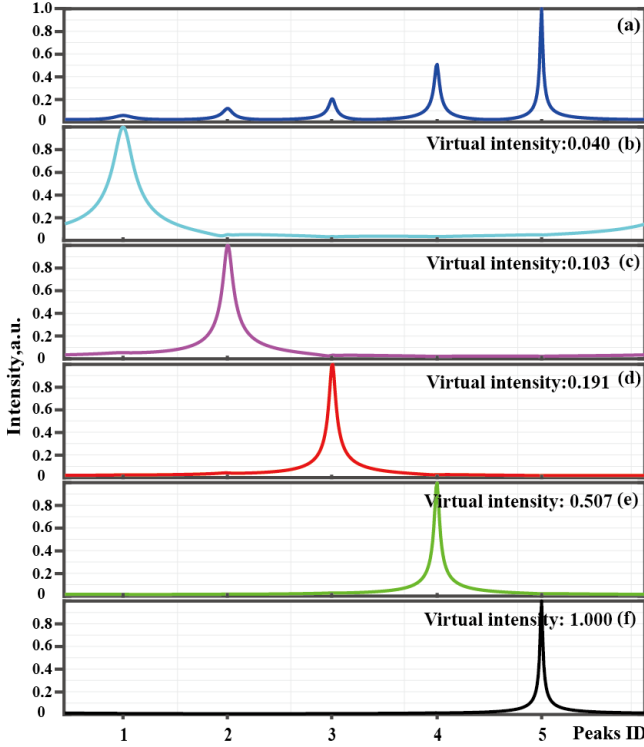


Fig. 2. Virtual peaks of a spectrum. (a) the original spectrum with 5 physical peaks, (b)-(f) virtual peaks that satisfies (a)=0.040×(b)+0.103×(c)+0.191×(d)+0.507×(e)+1.000×(f).

However, as the FID is a superimposed signal of these exponentials (or peaks), mining each exponential function (single peak) is not easy. We tend to SVD since there exists one-to-one correspondence between the VIP and the physical peak in this specific example, although some details of peaks that are marked by array may be slightly different. In general, one-to-one correspondence is hard since the SVD enforces the orthogonality of each column (and row) in the rank-1 matrix. Even though, these VIPs are empirically observed to carry most spectral information, such as the central frequency and lineshape of each peak (Figure 2). Besides, the linear combination of all VIPs is equal to the original physical spectrum, implying that information is not lost in the VIP decomposition. Therefore, VIP can be used to incorporate prior knowledge of a reference spectrum.

B. Self-learning of Virtual Peaks

How to learn reliable VIPs is another issue for the reconstruction since the fully sampled FID is not available in NUS. Here, we suggest to divide VIPs into strong and weak peaks according to their virtual intensities. This process is relatively easy since the virtual intensity, i.e. the singular value, is can be obtained with SVD on the Hankel matrix. In practice, we observe that strong VIPs are much more reliable than the weak ones.

As shown in Figure 3, we use Ω to denote the prior VIP information of strong peaks, and $\bar{\Omega}$ to represent the rest of peaks. Then, $\mathbf{A}=\mathbf{A}_\Omega \cup \mathbf{A}_{\bar{\Omega}}$ (and $\mathbf{B}=\mathbf{B}_\Omega \cup \mathbf{B}_{\bar{\Omega}}$) where \mathbf{A}_Ω (and \mathbf{B}_Ω) are the first p ($p \leq P$) columns and $\mathbf{A}_{\bar{\Omega}}$ (and $\mathbf{B}_{\bar{\Omega}}$) are the rest $N-p$ columns of \mathbf{A} (and \mathbf{B}). It should be noted that the first p columns correspond to the subspace for the largest p

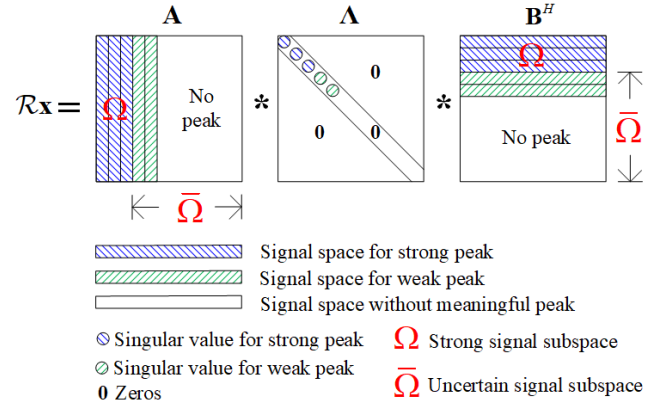


Fig. 3. Illustration on utilizing the reliable VIP from strong peaks.

singular values stored in Λ . Thus, the p is a parameter that determines the number of prior strong peaks. How this parameter affects the reconstruction was discussed in Section IV. B. Next, we will introduce where learn VIP, how to learn VIP and how to utilize reliable VIP.

Where to learn VIP? As the FID is undersampled, a reasonable solution is to utilize state-of-the-art reconstruction methods, such as compressed sensing [18] or low-rank [21], to obtain a good reference spectrum. Surprisingly, in practice, we found that the proposed method is insensitive to initial reference if the VIP is updated several times (See Section IV. A). Here, we simply choose the spectrum, which is reconstructed by filling zeros into the unsampled data points, as the initial reference, to avoid using multiple algorithms.

Now, the VIP is available for reconstruction. By introducing the VIP into the reconstruction model, the difficulty of solving the reconstruction problem will be reduced since fewer degrees of freedom for spectral peaks need to be estimated implicitly. Taking Figure 4 as a toy example, under an extremely high acceleration factor of 12.5, if this information taken by VIP is accurate, distorted peaks (peaks 1 and 2) can be reconstructed very faithfully, implying that the VIP has a strong ability to take prior information. Even when choosing the zero-filling spectrum as the reference, by learning the three strongest VIPs from the reference then updating references and then learning the information again, the challenging low-intensity peaks will be restored very well (Figure 4(d) and 4(e)).

C. Reconstruction Model of VIP

The proposed model is defined to feed the VIP information Ω of strong peaks into reconstruction as follows:

$$\min_{\mathbf{x}} \|\mathcal{R}\mathbf{x}\|_* - Tr(\mathbf{A}_\Omega^H \mathcal{R}\mathbf{x}\mathbf{B}_\Omega) + \frac{\lambda}{2} \|\mathbf{y} - \mathcal{U}\mathbf{x}\|_2^2, \quad (6)$$

where $\mathbf{x} \in \mathbb{C}^{2N+1}$ is the FID to be reconstructed, $\mathbf{y} \in \mathbb{C}^M$ are the acquired FID data, \mathcal{U} is an undersampling operator, and $\|\cdot\|_2$ represents the l_2 norm and λ is a parameter to balance the two terms, $\|\cdot\|_*$ represents the nuclear norm (sum of singular values), $Tr(\cdot)$ is a trace function (sum of the main diagonal elements), the superscript H denotes the Hermitian transpose. Ideally, if the VIP of strong peaks is accurate, the $\mathbf{A}_\Omega^H \mathcal{R}\mathbf{x}\mathbf{B}_\Omega$ will be a rank P diagonal matrix since both $\mathbf{A}_\Omega^H \mathbf{A}_\Omega$ and $\mathbf{B}_\Omega^H \mathbf{B}_\Omega$ will be the identity matrix. Thus, $Tr(\mathbf{A}_\Omega^H \mathcal{R}\mathbf{x}\mathbf{B}_\Omega)$ sums up the largest p singular values, i.e. virtual intensities. In other words,

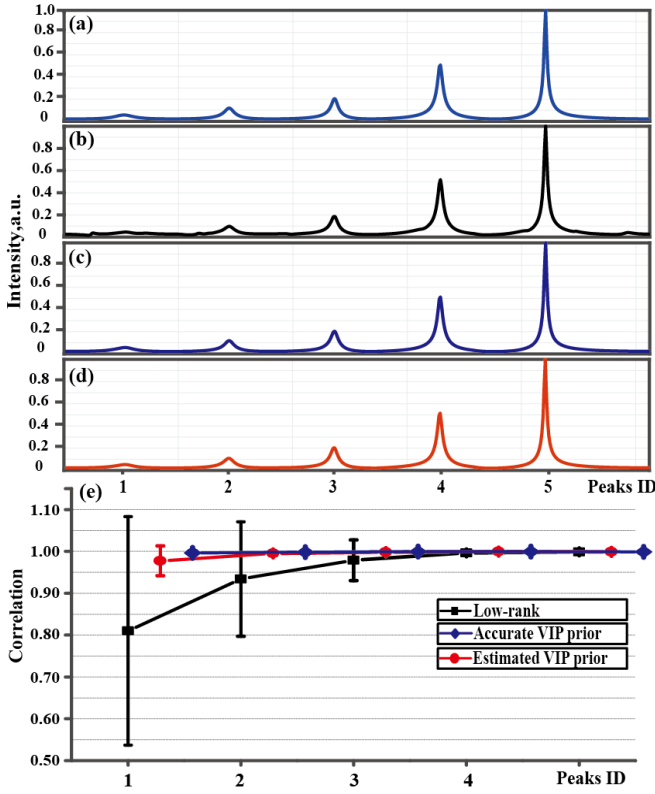


Fig. 4. Reconstruction of 5 peaks spectrum and peak intensity correlations for the reconstructed spectra when the sampled data is 8% of the fully sampled data. (a) is the original physical spectrum; (b) is reconstructed by low-rank; (c) is reconstructed with accurate prior of five VIPs (virtual intensity is not prior); (d) is reconstructed by the 3 most reliable, e.g. the highest three, VIPs; (e) is the peak intensity correlations of each peak. Note: The black, red and blue lines represent reconstructions by the low-rank, the proposed self-learned (self-learning) VIP method, and ideally accurate VIPs, respectively. The error bars are standard deviations of correlations over 100 sampling trials. A smaller bar indicates more robust reconstruction under different NUS trials.

$Tr(\mathbf{A}_{\Omega}^H \mathcal{R} \mathbf{x} \mathbf{B}_{\Omega})$ defines the nuclear norm [29], which is considered as a convex measure for the number of peaks of strong peaks [21]. Similarly, if the $\bar{\Omega}$ is accurate, then $\mathbf{A}_{\bar{\Omega}}^H \mathcal{R} \mathbf{x} \mathbf{B}_{\bar{\Omega}}$ will be of rank $P-p$ and the $Tr(\mathbf{A}_{\bar{\Omega}}^H \mathcal{R} \mathbf{x} \mathbf{B}_{\bar{\Omega}})$ will be an indicator of the number of weak peaks, i.e. $P-p$. Therefore, the model tries to find the minimal number of weak peaks with the prior knowledge of VIP.

This proposed model is also inspired by the truncated nuclear norm regularization in general matrix completion [30] and but we are solving a new reconstruction problem of missing data recovery of exponential functions. Besides, we have provided a clear interpretation of prior VIP information in NMR reconstruction, verified the performance on biological spectrum and implemented cloud computing platform for the algorithm.

D. Numerical Algorithm

In the NUS reconstruction, we suggest estimating the \mathbf{A}_{Ω} (and \mathbf{B}_{Ω}) from an initial solution \mathbf{x}_0 and obtain the initial \mathbf{A}_{Ω} (and \mathbf{B}_{Ω}), denoted as $\mathbf{A}_{\Omega,0}$ (and $\mathbf{B}_{\Omega,0}$), from the first p columns from \mathbf{A} (and \mathbf{B}) in $\mathcal{R} \mathbf{x}_0 = \mathbf{A} \mathbf{A} \mathbf{B}^H$. Then, the VIP

prior is further improved to $\mathbf{A}_{\Omega,l}$ (and $\mathbf{B}_{\Omega,l}$) with an updated solution \mathbf{x}_l at the l^{th} iterations in the implementation. Therefore, the proposed method includes two layers of loops. The outer loop updates the VIPs, the inner loop reconstructs signal under the given VIPs.

For the given $\mathbf{A}_{\Omega,l}$ and $\mathbf{B}_{\Omega,l}$, the model is solved with the Alternating Direction Method of Multipliers (ADMM) [31]. The augmented Lagrange of Eq. (6) is

$$G(\mathbf{x}, \mathbf{Z}, \mathbf{D}) = \|\mathbf{Z}\|_* - Tr(\mathbf{A}_{\Omega,l}^H \mathbf{Z} \mathbf{B}_{\Omega,l}) + \langle \mathbf{D}, \mathcal{R} \mathbf{x} - \mathbf{Z} \rangle + \frac{\beta}{2} \|\mathcal{R} \mathbf{x} - \mathbf{Z}\|_F^2 + \frac{\lambda}{2} \|\mathcal{U} \mathbf{x} - \mathbf{y}\|_2^2, \quad (7)$$

where \mathbf{D} is a dual variable, and $\langle \cdot, \cdot \rangle$ is the inner product in the Hilbert space of matrices, $\|\cdot\|_F$ means the Frobenius norm and $\beta > 0$ is a parameter.

Eq. (7) is alternately solved via the following sub-problems until the algorithm converges:

$$\begin{cases} \mathbf{x}^{k+1} = \arg \min_{\mathbf{x}} G(\mathbf{x}, \mathbf{Z}^k, \mathbf{D}^k) \\ \mathbf{Z}^{k+1} = \arg \min_{\mathbf{Z}} G(\mathbf{x}^{k+1}, \mathbf{Z}, \mathbf{D}^k). \\ \mathbf{D}^{k+1} = \mathbf{D}^k + (\mathcal{R} \mathbf{x}^{k+1} - \mathbf{Z}^{k+1}) \end{cases} \quad (8)$$

1) Fixing \mathbf{D}^k and \mathbf{Z}^k , \mathbf{x}^{k+1} is obtained by solving

$$\min_{\mathbf{x}} \langle \mathbf{D}^k, \mathcal{R} \mathbf{x} - \mathbf{Z}^k \rangle + \frac{\beta}{2} \|\mathcal{R} \mathbf{x} - \mathbf{Z}^k\|_F^2 + \frac{\lambda}{2} \|\mathbf{y} - \mathcal{U} \mathbf{x}\|_2^2, \quad (9)$$

whose solution is

$$\mathbf{x}^{k+1} = (\lambda \mathcal{U}^* \mathcal{U} + \beta \mathcal{R}^* \mathcal{R})^{-1} \left(\lambda \mathcal{U}^* \mathbf{y} + \beta \mathcal{R}^* \left(\mathbf{Z}^k - \frac{\mathbf{D}^k}{\beta} \right) \right), \quad (10)$$

where the superscript $*$ denotes the adjoint operator.

2) Fixing \mathbf{D}^k and \mathbf{x}^{k+1} , \mathbf{Z}^{k+1} is obtained by solving

$$\min_{\mathbf{Z}} \|\mathbf{Z}\|_* - Tr(\mathbf{A}_{\Omega,l}^H \mathcal{R} \mathbf{x} \mathbf{B}_{\Omega,l}) + \langle \mathbf{D}^k, \mathcal{R} \mathbf{x} - \mathbf{Z} \rangle + \frac{\beta}{2} \|\mathcal{R} \mathbf{x} - \mathbf{Z}\|_F^2, \quad (11)$$

whose solution is

$$\mathbf{Z}^{k+1} = \mathcal{D}_{1/\beta} \left(\mathcal{R} \mathbf{x}^{k+1} + \frac{1}{\beta} (\mathbf{A}_{\Omega,l} \mathbf{B}_{\Omega,l}^H + \mathbf{D}^k) \right), \quad (12)$$

where the $\mathcal{D}_{1/\beta}$ is a singular thresholding operator [29] on a matrix with threshold $1/\beta$.

3) Fixing \mathbf{Z}^{k+1} and \mathbf{x}^{k+1} , update \mathbf{D}^{k+1} according to

$$\mathbf{D}^{k+1} = \mathbf{D}^k + (\mathcal{R} \mathbf{x}^{k+1} - \mathbf{Z}^{k+1}). \quad (13)$$

Thus, the alternating in the three sub-equations of Eq. (8) stops if the number of iterations k reaches the maximal number K or the $\eta_{k+1} = \|\mathbf{x}^{k+1} - \mathbf{x}^k\| / \|\mathbf{x}^k\|$ normalized successive difference is smaller than a given tolerance $\eta_{\text{tol}} = 10^{-5}$.

The overall algorithm is summarized in Table I, including updating VIP subspaces \mathbf{A}_{Ω} and \mathbf{B}_{Ω} in the outer loop and solving the solution \mathbf{x} in the inner loop.

TABLE I THE NUMERICAL ALGORITHM FOR SOLVING THE PROPOSED METHOD	
Initialization: Input \mathbf{y} , \mathcal{R} , \mathcal{U} , set outer maximal iterations times $L=5$ of updating as $\mathbf{A}_{\Omega,l}$ and $\mathbf{B}_{\Omega,r}$, convergence condition $\eta_{\text{tol}} = 10^{-5}$, and inner maximal number of iterations $K = 10^3$. Initialize the solution $\mathbf{x}_0 = \mathcal{U}^* \mathbf{y}$, the dual variable $\mathbf{D}_0 = \mathbf{1}$, the number of iterations $k = 0$, $\eta_0 = 1$.	
Main:	
While ($\eta \geq \eta_{\text{tol}}$) or ($l < L$), do	
1)	Estimate $\mathbf{A}_{\Omega,l}$ and $\mathbf{B}_{\Omega,l}$ from the first p columns of \mathbf{A}_l and \mathbf{B}_l , respectively, where \mathbf{A}_l and \mathbf{B}_l obey the singular value decomposition $\mathcal{R} \mathbf{x}_l = \mathbf{A}_l \mathbf{\Lambda} \mathbf{B}_l^H$.
While ($\eta_k \geq \eta_{\text{tol}}$) or ($k < K$), do	
a)	Update \mathbf{x}^{k+1} according to Eq. (10);
b)	Update \mathbf{Z}^{k+1} according to Eq. (12);
d)	Update \mathbf{D}^{k+1} according to Eq. (13);
e)	Compute $\eta^{k+1} = \frac{\ \mathbf{x}^{k+1} - \mathbf{x}^k\ }{\ \mathbf{x}^k\ }$ and $k \leftarrow k + 1$;
End while	
2)	Set $k = 0$, $\eta^k = 1$ and $l \leftarrow l + 1$;
3)	Update $\mathbf{x}_{l+1} \leftarrow \mathbf{x}^{k+1}$, $\eta_{l+1} = \frac{\ \mathbf{x}_{l+1} - \mathbf{x}_l\ }{\ \mathbf{x}_l\ }$;
End for	
Output: The reconstructed FID $\hat{\mathbf{x}} \leftarrow \mathbf{x}_{l+1}$.	

III. RESULTS

A. Experimental Setup and Evaluation Criteria

In this section, the performance of the proposed method is validated on realistic NMR data under the Poisson NUS [8]. The experimental details are summarized in Supplement S7. To avoid ambiguity when spectrometers are in different magnet strengths, the parts per million (ppm) is defined as the unit of chemical shift [32] according to:

$$\text{chemical shift(ppm)} = \frac{f_{\text{sample}} - f_{\text{ref}}}{f_{\text{spec}}} \times 10^6, \quad (14)$$

where f_{sample} is the resonance frequency of the sample, f_{ref} is the absolute resonance frequency of a standard compound measured in the same magnetic field and f_{spec} is the frequency of magnetic field strength of spectrometer.

To evaluate the quality of the reconstruction, we use the squared of the Pearson correlation coefficient (R^2) to measure the correlation between the reconstructed spectrum $\hat{\mathbf{x}}$ and the fully sampled spectrum \mathbf{x} . The R^2 is defined as follows:

$$R^2(\hat{\mathbf{x}}, \mathbf{x}) = \left(\frac{\text{cov}(\hat{\mathbf{x}}, \mathbf{x})}{\sigma_{\hat{\mathbf{x}}} \sigma_{\mathbf{x}}} \right)^2, \quad (15)$$

where $\text{cov}(\cdot)$ and σ denotes the covariance and standard deviation, respectively.

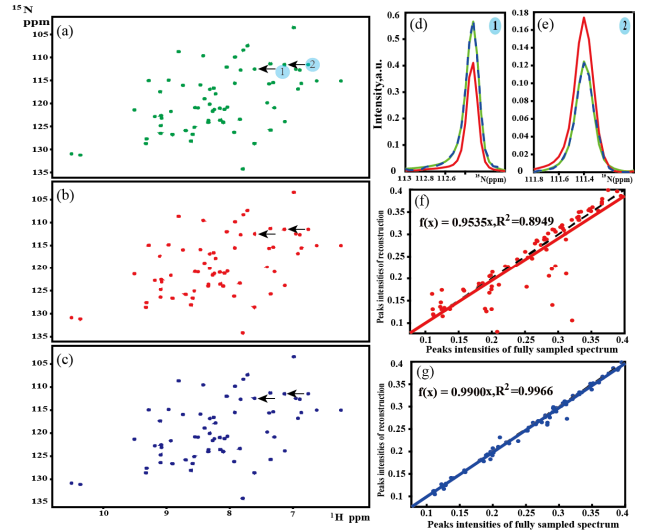


Fig. 5. Reconstruction of 2D HSQC spectra of the protein GB1. (a) is the fully sampled reference spectrum, (b) and (c) are reconstructed spectra from 15% NUS data by the low-rank and the proposed VIP method, respectively, (d) and (e) are zoomed out 1D ^{15}N traces, and the green, red and blue lines represent the reference, low-rank and VIP reconstructed spectra, respectively. (f) and (g) are estimated with partial peaks of low intensities at a range of [0, 0.4] using the low-rank and VIP, respectively.

B. Reconstruction of Realistic NMR Data

The first NUS reconstruction is conducted on a 2D HSQC spectrum of a protein GB1 with a limited 15% of fully sampled data. Figure 5(a)-(c) show that both low-rank and the proposed VIP can reconstruct most spectral peaks. However, a close look at the low-intensity peaks (Figure 5(d) and 5(e)) clearly show that the low-rank method may reduce or increase the intensities, while the VIP method achieves much higher fidelity peaks. The correlation of low-intensity peaks is greatly increased from 0.89 in low-rank to 0.99 in VIP. Better reconstructions obtained with VIP are also observed on another two NMR spectra, including a ^1H - ^{15}N best-TROSY spectrum and a ^1H - ^{15}N HSQC spectrum of Ubiquitin (See Supplement S2).

C. Quantitative Measures on Internuclear Distances

Quantitative measures on internuclear distances are analysed on a 2D ^1H - ^1H NOESY spectrum of strychnine (Figure 6) [13, 14]. In the reconstruction from 20% NUS data, some cross-peaks (marked with arrows 1 and 2 in Figure 7(b)), which are missed or weakened by low-rank, are preserved well by the VIP method (Figure 7(c)). The correlation of peak intensity indicates that the VIP method can improve the fidelity of low-intensity peaks (Figure S3-1 of Supplement S3).

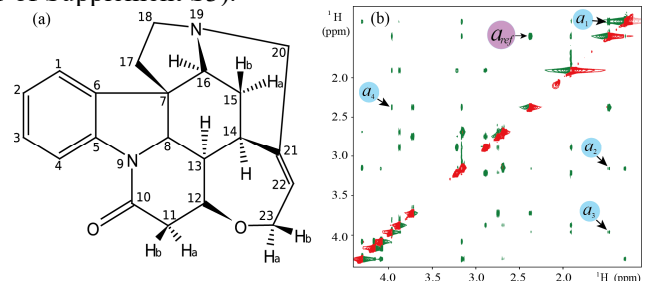


Fig. 6. Strychnine [13, 14]. (a) Molecular structure, (b) the fully sampled spectrum.

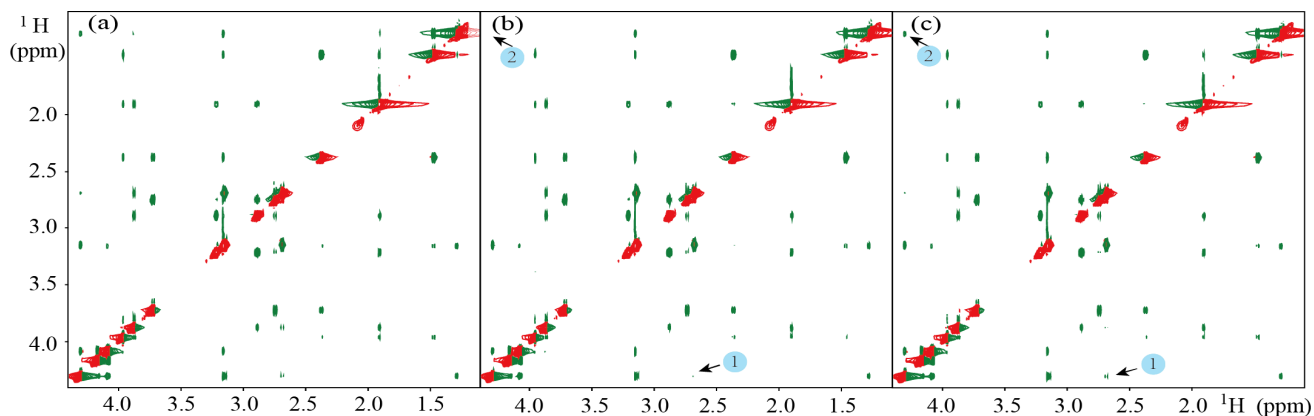


Fig. 7. Reconstruction of a 2D ^1H - ^1H NOESY spectra of strychnine. (a) The full sampled spectrum, (b) and (c) are reconstructed spectra by the low-rank and VIP, respectively. Note: 20% data are sampled in the NUS. Negative and positive peaks are represented with green and red colors, respectively.

We further analyze a quantitative measure, the internuclear distance, which is important for computing molecular structure. The distance is defined as

$$d = d_{ref} \left(\frac{a}{a_{ref}} \right)^{\frac{1}{6}} \quad (16)$$

where $d_{ref}=1.76 \text{ \AA}$ is a reference distance for internuclear H15a-H15b [13, 14], a_{ref} is the integral of the cross peak (marked as a_{ref} in Figure 6(b)) that belongs to the internuclear H15a-H15b, a is the integral of target cross-peaks (marked as a_1, a_2, a_3, a_4 in Figure 6(b)). Table II implies that VIP leads to the closest distances to those of the fully sampled spectrum.

TABLE II
SELECTED INTERNUCLEAR DISTANCES FROM THE NOESY SPECTRA OF STRYCHNINE (UNIT: \AA)

No. of points	Fully sampled spectrum	NUS reconstruction	
		Low-rank	VIP
H15a-H15b	1.76	1.76	1.76
H13-H15a	2.25	2.08	2.28
H14-H15a	2.68	2.30	2.74
H16-H15a	2.54	3.38	2.63
H15b-H16	2.47	2.16	2.54

Note: The integral of peak is reported in Supplement S3.

D. Quantitative Measures on the Relative Concentration

Quantitative measures on the relative concentration are analysed on a mixture of 3 metabolites, including D-Glucose, β -Alanine and Valine (Figure S4-1). A series of HSQC_i ($i=1,2,3$) spectra (Figure S4-2) are separately reconstructed by using 15% NUS data and then extrapolated back to a time-zero HSQC (HSQC₀) spectrum. As the concentration of an individual metabolite is proportional to the peak intensity [33], the concentration measurement for an individual metabolite can be improved by averaging the intensities of multiple cross-peaks that belongs to the same metabolite [34]. A relative concentration of each metabolite is calculated as the ratio of its integration over the integration of the Valine (See Supplement S4 for more details).

Table III indicates that VIP provides the closest concentration to that of the fully sampled spectrum.

TABLE III
RELATIVE CONCENTRATIONS OF METABOLITES IN THE MIXTURE

Metabolites	Fully sampled spectrum	NUS reconstruction	
		Low-rank	VIP
Valine	1	1	1
β -Alanine	2.38	2.54	2.40
D-Glucose	4.60	4.84	4.50

Note: The concentration for each metabolite is improved by averaging the intensities of multiple, non-overlapping cross peaks assigned to that metabolite (Supplement S4). The closer the concentration to the full sampling spectrum peak is, the more accurate the reconstruction method is.

E. Cloud Computing

Cloud computing is a state-of-the-art technology that is generally web-based and easily accessible at any time. Here, we develop XCloud-VIP, a cloud computing platform for spectra reconstruction with the proposed method. The browser/server architecture of XCloud-VIP is shown in Figure 8. The whole processing flow is easy to use for NMR researchers: 1) Upload and pre-process raw data online; 2) Set the number of prior strong peaks and other reconstruction parameters; 3) Start online reconstruction; 4) Download the reconstructed data and show the spectrum. The manual, demo data, and post-processing scripts are accessible via the URL address and test accounts that are shared in Table IV.

The spectra parameters and the reconstruction time are summarized in Table V. The configuration of the local server includes two E5-2650v4 CPUs (12 cores) and 160 GB RAM. The cloud computing configuration is a CPU with 64 cores and 256 GB RAM. Table V shows that the cloud computing enables shorter reconstruction time.

TABLE IV
TEST ACCOUNTS ON XCLOUD-VIP

User account	Password
CSG_test001	TEST@CSG01
CSG_test002	USER_test02
CSG_test003	SERVICE_CSGtest03

Note: The website of XCloud-VIP is <http://36.134.71.5:2345>

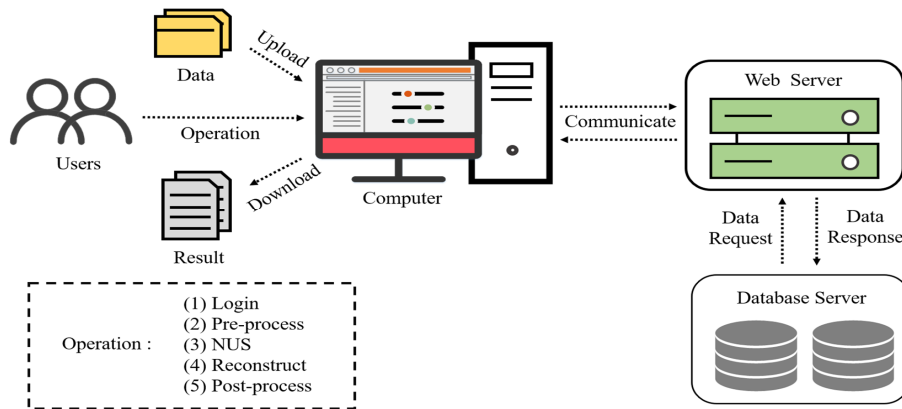


Fig. 8. A system framework of the XCloud-VIP.

TABLE V
IMPORTANT SPECTRAL PARAMETERS AND RECONSTRUCTION TIME

Spectra Type	Protein	Spectra size for reconstruction ($t_2 \times t_1$)	References	Sampling Rate	Reconstruction Time (s)	
					Local	Cloud
HSQC	GB1	1146 × 170	Fig. 5	15%	173.02	118.02
NOESY	/	2048 × 256	Fig. 7	20%	240.68	160.84
TROSY	Ubiquitin	682 × 128	Fig. S2-1(b-1)	20%	47.79	33.54
HSQC	Ubiquitin	1024 × 98	Fig. S2-1(a-1)	20%	27.76	21.62
HSQC (3 mixture)	/	1024 × 256	Fig. S4-1	15%	93.21	63.54

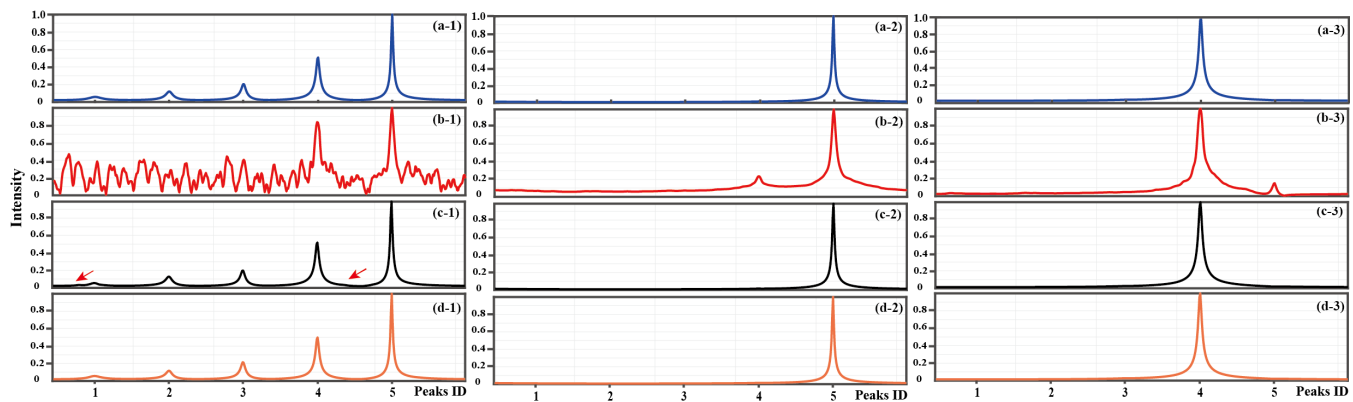


Fig. 9. Effect of updating VIP when the zero-filling spectrum is chosen as the initial reference. (a-1) the full sampled spectrum; (b-1), (c-1) and (d-1) are intermediate 1st, 2nd and 3rd reconstructions used to learn the VIP, respectively; (a-2) and (a-3) are accurate VIP learnt from the two strongest physical peaks in the fully sampled spectra in (a-1), respectively; (b-2) and (b-3) are estimated VIPs learnt from the two strongest peaks in the 1st intermediate reconstruction in (b-1); (c-2) and (c-3) are estimated VIPs learnt from the two strongest peaks in the 1st intermediate reconstruction in (c-1); (d-2) and (d-3) are estimated VIPs learnt from the two strongest peaks in the 1st intermediate reconstruction in (d-1). Note: 8% of fully sampled data were used in the reconstruction. All the reconstructions are accomplished by the VIP method with the number of strong peaks $p=3$.

IV. DISCUSSIONS

A. Discussion on Initial Reference Spectra

The VIPs (Figures 9(b-2) and (b-3)), learnt from the initial zero-filling spectrum (Figure 9(b-1)), take spectral information, such as the central frequency, and lead to nice reconstruction (Figure 9(c-1)). However, these initial VIPs still have distortion, comparing with the accurate VIPs (Figures 9(a-2) and (a-3)), and lead to distortions in the reconstruction spectra (marked with arrays in Figure 9(c-1)). By further learning the VIP from the intermediate reconstruction (Figure 9(c-1)), the lineshapes of VIP have been greatly improved (Figures 9(c-2) and (c-3)), and high-quality spectra (Figure 9(d-1)) have been reconstructed. These observations imply that even starting from

the zero-filling spectrum, the VIP becomes more reliable if multiple times of reference updating and VIP reconstructions are allowed. In practice, we found 5 times of learning is sufficient.

B. Discussion on the Number of Prior Strong Peaks

To verify the sensitivity to the number of prior strong peaks (p), VIP reconstructions of synthetic data are discussed here. Figures 10(a) and (b) show that the VIP improves the reconstruction even when only a single strong peak is introduced. Best reconstruction performance is obtained when the number of strong peaks (p) is equal to the number of true peaks (P), i.e. $p=P=5$. The closer to the number of true peaks (P) is, the better the performance is.

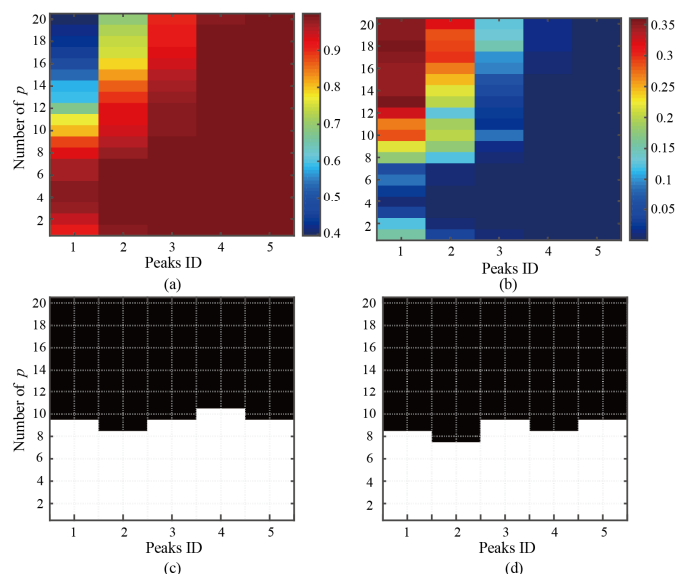


Fig. 10. The peak intensity correlation versus the number of strong peaks (p). (a) and (b) are the average and standard deviation for peak intensity correlation for each peak, respectively. The white region of (c) and (d) indicate a better performance of VIP than that of the low-rank method. Note: Detailed correlations are reported in Table S7-1. The color bar in (a) and (b) indicates the peak intensity correlation. White color in (c) (or (d)) indicates a higher average (or lower standard deviation) obtained with VIP than that of the low-rank method. The peaks 1~5 denote the peaks from the left to the right in Figure 2(a) of the main text. 8% of the fully sampled data is used in the NUS. (More detailed criteria can be found in Supplement S6)

Figures 10(c) and (d) indicate that an improved performance always holds if the number of strong peaks (p) is set to in the range $p \in [1, 2P]$. In practice, one can always assume that the exists at least one peak in the spectrum to obtain better reconstructions.

To sum up, VIP always outperforms the compared method if the number of strong peaks is between one and 2 times of the number of true peaks, indicating the robustness of this parameter.

V. CONCLUSION

In this study, we propose a self-learning virtual peaks approach to realize high-quality NMR spectra reconstructions under high acceleration factors and set up an easy-accessible cloud computing platform, XCloud-VIP, for the proposed method. Virtual peaks incorporate the prior spectral information, such as the central frequency and peak lineshape into reconstructions. The proposed method can reconstruct reliable low-intensity peaks, and obtain faithful quantitative measures, such as internuclear distances and concentration of mixtures. Thus, the proposed method enables higher factors of NMR data acquisition, which may significantly promote time-consuming NMR applications such as time-resolved experiments, real-time experiments, or *in vivo* studies of short-lived systems. Future work could utilize the Vandermonde Hankel matrix decomposition [9] to separate extremely close and overlapped peaks, and maintain high-fidelity reconstruction for more accurate quantitative measures.

ACKNOWLEDGEMENT

The authors are grateful to Hengfa Lu for plotting some figures, Prof. Vladislav Orekhov for valuable discussions and Chunyan Xiong, Xinlin Zhang, Huiting Liu and Jinyu Wu for valuable suggestions.

REFERENCES

- [1] J. Stanek, R. Augustyniak, and W. Koźmiński, "Suppression of sampling artefacts in high-resolution four-dimensional NMR spectra using signal separation algorithm," *J. Magn. Reson.*, vol. 214, pp. 91-102, 2012.
- [2] M. Mobli, and J. C. Hoch, "Nonuniform sampling and non-fourier signal processing methods in multidimensional NMR," *Prog. Nucl. Magn. Reson. Spectrosc.*, vol. 83, pp. 21-41, 2014.
- [3] S. Robson, H. Arthanari, S. G. Hyberts, and G. Wagner, "Nonuniform sampling for NMR spectroscopy," *Methods Enzymol.*, vol. 614, pp. 263-291, 2019.
- [4] B. E. Coggins, R. A. Venters, and P. Zhou, "Radial sampling for fast NMR: concepts and practices over three decades," *Prog. Nucl. Magn. Reson. Spectrosc.*, vol. 57, no. 4, pp. 381-491, 2010.
- [5] D. J. Holland, M. J. Bostock, L. F. Gladden, and D. Nietlispach, "Fast multidimensional NMR spectroscopy using compressed sensing," *Angew. Chem. Int. Edit.*, vol. 50, no. 29, pp. 6548-6551, 2011.
- [6] K. Kazimierczuk, and V. Y. Orekhov, "Accelerated NMR spectroscopy by using compressed sensing," *Angew. Chem. Int. Edit.*, vol. 123, no. 24, pp. 5670-5673, 2011.
- [7] X. Qu, D. Guo, X. Cao, S. Cai, and Z. Chen, "Reconstruction of self-sparse 2D NMR spectra from undersampled data in the indirect dimension," *Sensors*, vol. 11, no. 9, pp. 8888-8909, 2011.
- [8] S. G. Hyberts, A. G. Milbradt, A. B. Wagner, H. Arthanari, and G. Wagner, "Application of iterative soft thresholding for fast reconstruction of NMR data non-uniformly sampled with multidimensional Poisson Gap scheduling," *J. Biomol. NMR*, vol. 52, no. 4, pp. 315-327, 2012.
- [9] J. Ying, J.-F. Cai, D. Guo, G. Tang, Z. Chen, and X. Qu, "Vandermonde factorization of Hankel matrix for complex exponential signal recovery—application in fast NMR spectroscopy," *IEEE Trans. Signal. Process.*, vol. 66, no. 21, pp. 5520-5533, 2018.
- [10] X. Qu, Y. Huang, H. Lu, T. Qiu, D. Guo, V. Y. Orekhov, and Z. Chen, "Accelerated nuclear magnetic resonance spectroscopy with deep learning," *Angew. Chem. Int. Edit.*, vol. 59, no. 26, pp. 10297-10300, 2019.
- [11] D. Chen, Z. Wang, D. Guo, V. Y. Orekhov, and X. Qu, "Review and prospect: deep learning in nuclear magnetic resonance spectroscopy," *Chem-Eur. J.*, vol. 26, pp. 10391-10401, 2020.
- [12] K. H. Jin, D. Lee, and J. C. Ye, "A general framework for compressed sensing and parallel MRI using annihilating filter based low-rank Hankel matrix," *IEEE Trans. Comput. Imag.*, vol. 2, no. 4, pp. 480-495, 2016.
- [13] C. P. Butts, C. R. Jones, E. C. Towers, J. L. Flynn, L. Appleby, and N. J. Barron, "Interproton distance determinations by NOE—surprising accuracy and precision in a rigid organic molecule," *Org. Biomol. Chem.*, vol. 9, no. 1, pp. 177-184, 2011.
- [14] R. Dass, P. Kasprzak, W. Koźmiński, and K. Kazimierczuk, "Artifacts in time-resolved NUS: A case study of NOE build-up curves from 2D NOESY," *J. Magn. Reson.*, vol. 265, pp. 108-116, 2016.
- [15] X. Qu, T. Qiu, D. Guo, H. Lu, J. Ying, M. Shen, B. Hu, V. Orekhov, and Z. Chen, "High-fidelity spectroscopy reconstruction in accelerated NMR," *Chem. Commun.*, vol. 54, no. 78, pp. 10958-10961, 2018.
- [16] F. Lam, and Z.-P. Liang, "A subspace approach to high-resolution spectroscopic imaging," *Magn. Reson. Med.*, vol. 71, no. 4, pp. 1349-1357, 2014.
- [17] J. He, Q. Liu, A. G. Christodoulou, C. Ma, F. Lam, and Z.-P. Liang, "Accelerated high-dimensional MR imaging with sparse sampling using low-rank tensors," *IEEE Trans. Med. Imag.*, vol. 35, no. 9, pp. 2119-2129, 2016.
- [18] M. Mayzel, K. Kazimierczuk, and V. Y. Orekhov, "The causality principle in the reconstruction of sparse NMR spectra," *Chem. Commun.*, vol. 50, no. 64, pp. 8947-8950, 2014.
- [19] J. C. Hoch, and A. S. Stern, "NMR data processing," *Phys. Med Biol.*, vol. 42, no. 3, pp. 611, 1997.
- [20] H. M. Nguyen, X. Peng, M. N. Do, and Z.-P. Liang, "Denoising MR spectroscopic imaging data with low-rank approximations," *IEEE Trans. Bio-Med. Eng.*, vol. 60, no. 1, pp. 78-89, 2013.
- [21] X. Qu, M. Mayzel, J.-F. Cai, Z. Chen, and V. Y. Orekhov, "Accelerated

- NMR spectroscopy with low-rank reconstruction," *Angew. Chem. Int. Edit.*, vol. 54, no. 3, pp. 852-854, 2015.
- [22] J. Ying, H. Lu, Q. Wei, J.-F. Cai, D. Guo, J. Wu, Z. Chen, X. Qu, "Hankel matrix nuclear norm regularized tensor completion for N-dimensional exponential signals," *IEEE Trans. Signal Process.*, vol. 65, no. 14, pp. 3702-3717, 2017.
- [23] G. Oh, B. Sim, H. Chung, L. Sunwoo, and J. C. Ye, "Unpaired deep learning for accelerated MRI using optimal transport driven cycleGAN," *IEEE Trans. Comput. Imag.*, vol. 6, pp. 1285-1296, 2020.
- [24] D. Guo, H. Lu, and X. Qu, "A fast low rank Hankel matrix factorization reconstruction method for non-uniformly sampled magnetic resonance spectroscopy," *IEEE Access*, vol. 5, pp. 16033-16039, 2017.
- [25] D. Guo, and X. Qu, "Improved reconstruction of low intensity magnetic resonance spectroscopy with weighted low rank Hankel matrix completion," *IEEE Access*, vol. 6, pp. 4933-4940, 2018.
- [26] H. Lu, X. Zhang, T. Qiu, J. Yang, J. Ying, D. Guo, Z. Chen, and X. Qu, "Low rank enhanced matrix recovery of hybrid time and frequency data in fast magnetic resonance spectroscopy," *IEEE Trans. Bio-Med. Eng.*, vol. 64, no. 5, pp. 809-820, 2018.
- [27] P. Koehl, "Linear prediction spectral analysis of NMR data," *Prog. Nucl. Magn. Reson. Spectrosc.*, vol. 34, no. 34, pp. 257-299, 1999.
- [28] T. Qiu, Z. Wang, H. Liu, D. Guo, and X. Qu, "Review and prospect: NMR spectroscopy denoising and reconstruction with low-rank Hankel matrices and tensors," *Magn. Reson. Chem.*, vol. 59, no. 3, pp. 324-345, 2021.
- [29] J.-F. Cai, E. J. Candès, and Z. Shen, "A singular value thresholding algorithm for matrix completion," *SIAM J. Optimiz.*, vol. 20, no. 4, pp. 1956-1982, 2010.
- [30] Y. Hu, D. Zhang, J. Ye, X. Li and X. He. "Fast and accurate matrix completion via truncated nuclear norm regularization," *IEEE Trans. Pattern Anal. Mach. Intell.*, vol. 35, no. 9, pp. 2117-2130, 2012.
- [31] S. Boyd, N. Parikh, E. Chu, B. Peleato, and J. Eckstein, "Distributed optimization and statistical learning via the alternating direction method of multipliers," *Found. Trends Mach. Learn.*, vol. 3, no. 1, pp. 1-122, 2011.
- [32] Z. Tu, Z. Wang, J. Zhan, Y. Huang, X. Du, M. Xiao, X. Qu, and D. Guo, "A partial sum of singular-value-based reconstruction method for non-uniformly sampled NMR spectroscopy," *IET Signal Process.*, vol. 15, no. 1, pp. 14-27, 2021.
- [33] K. Hu, J. J. Ellinger, R. A. Chylla, and J. L. Markley, "Measurement of absolute concentrations of individual compounds in metabolite mixtures by gradient-selective time-zero ^1H - ^{13}C HSQC with two concentration references and fast maximum likelihood reconstruction analysis," *Anal. Chem.*, vol. 83, no. 24, pp. 9352-9360, 2011.
- [34] K. Hu, W. M. Westler, and J. L. Markley, "Simultaneous quantification and identification of individual chemicals in metabolite mixtures by two-dimensional extrapolated time-zero ^1H - ^{13}C HSQC (HSQC₀)," *J. Am. Chem. Soc.*, vol. 133, no. 6, pp. 1662-1665, 2011.

Supplementary Information

XCloud-VIP: Virtual Peak Enables Highly Accelerated NMR Spectroscopy and Faithful Quantitative Measures

Di Guo ¹, Zhangren Tu ², Yi Guo ¹, Yirong Zhou ², Jian Wang ², Zi Wang ², Tianyu Qiu ², Min Xiao ³, Liubin Feng ⁴, Yuqing Huang ², Donghai Lin ⁴, Yongfu You ⁵, Amir Goldbourn ⁶, and Xiaobo Qu ^{*3}

- 1 Di Guo, Yi Guo are with the School of Computer and Information Engineering, Xiamen University of Technology, Xiamen 361024, China.
- 2 Zhangren Tu, Yirong Zhou, Jian Wang, Zi Wang, Tianyu Qiu, Yuqing Huang, Xiaobo Qu are with the Department of Electronic Science, Biomedical Intelligent Cloud R&D Center, Fujian Provincial Key Laboratory of Plasma and Magnetic Resonance, Xiamen University, Xiamen 361005, China.
- 3 Min Xiao are with the School of Opto-Electronic and Communication Engineering, Xiamen University of Technology, Xiamen 361024, China.
- 4 Liubin Feng, Donghai Lin are with the College of Chemistry and Chemical Engineering, Key Laboratory for Chemical Biology of Fujian Province, High-field NMR Center, Xiamen University, Xiamen 361005, China.
- 5 Yongfu You is with the China Mobile Group, Xiamen 361005, China.
- 6 Amir Goldbourn is with the School of Chemistry, Tel Aviv University, Tel Aviv 6997801, Israel.

**Corresponding author: quxiaobo@xmu.edu.cn*

Supplement S1: Methodology

1.1 The flowchart of the algorithm:

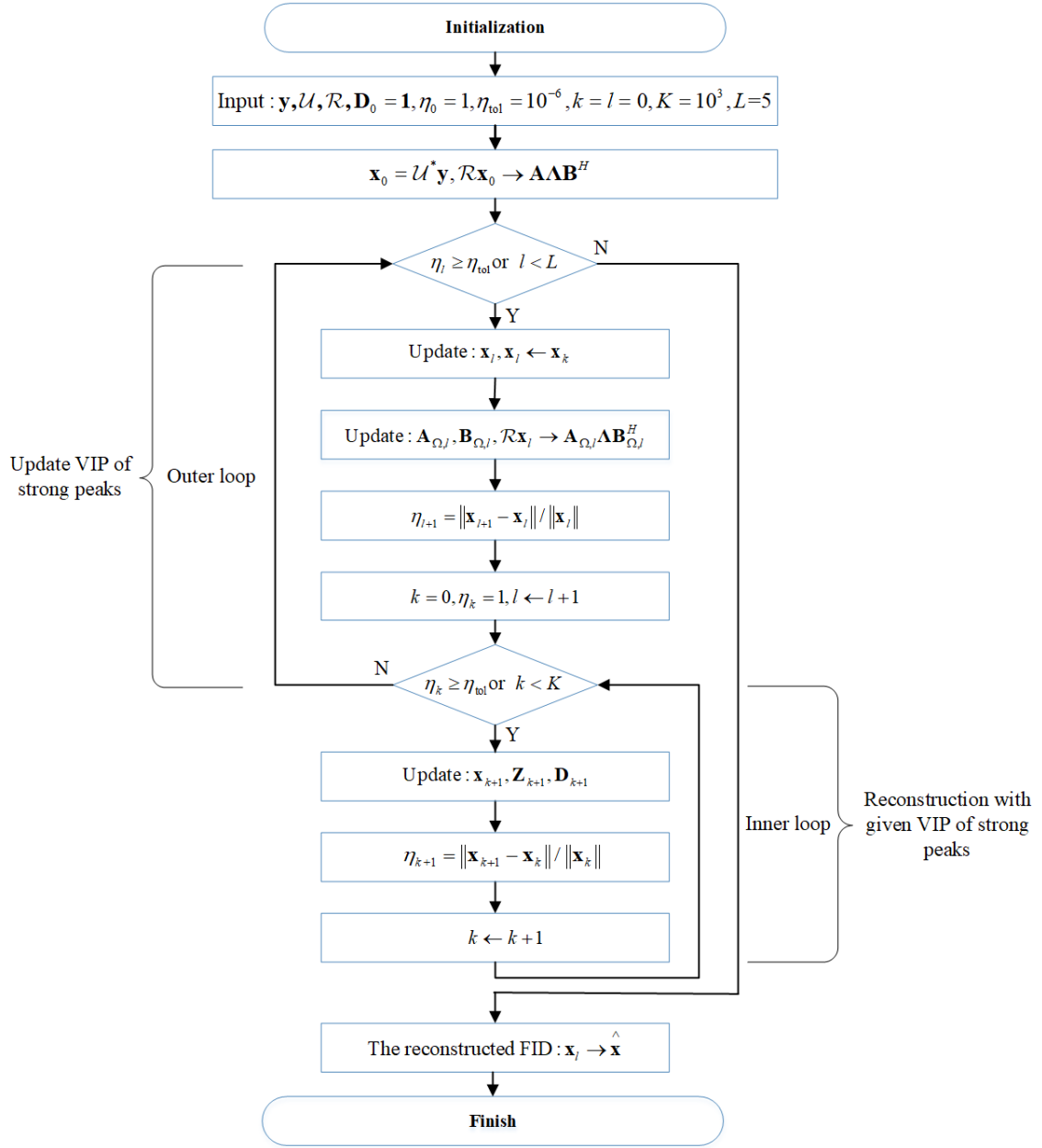


Figure S1-1. Flowchart of the proposed algorithm

S2. Results on other protein spectra

Reconstructed spectra and the analysis of the 2D ^1H - ^{15}N best-TROSY spectrum and ^1H - ^{15}N HSQC spectrum of Ubiquitin are reported in this section. The experiment is summarized in Supplement S7.

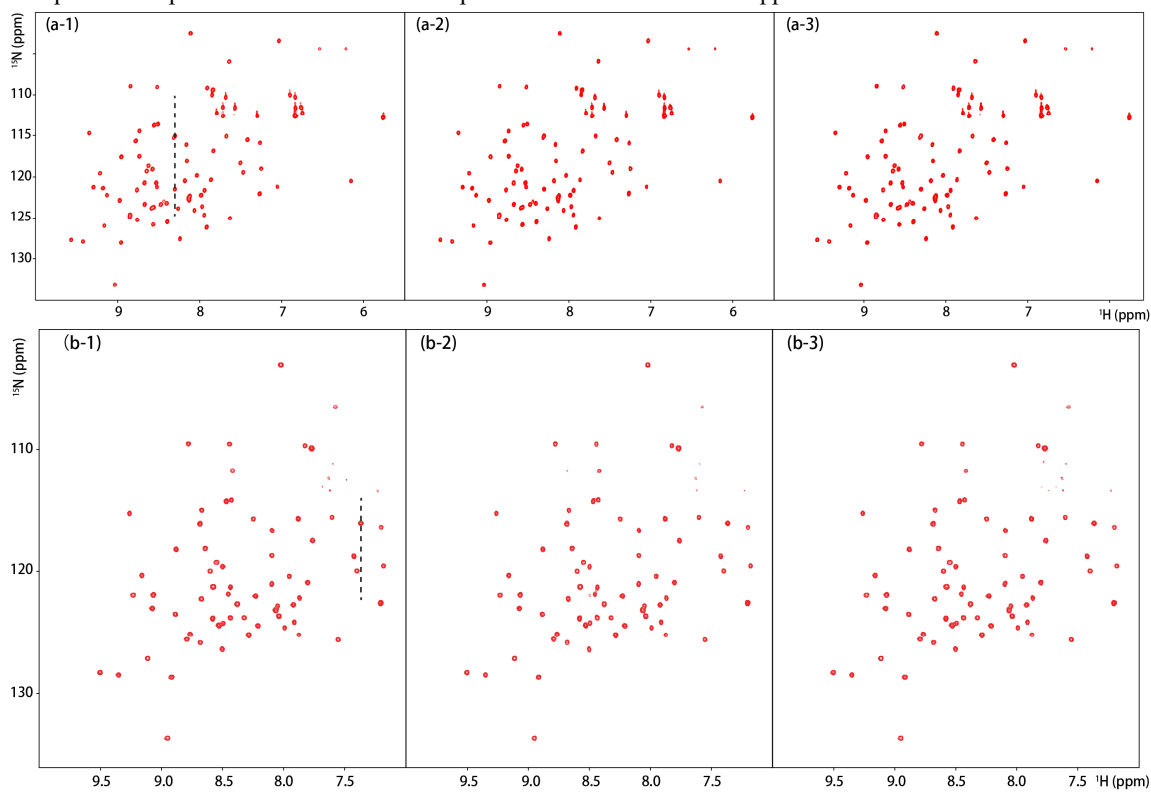


Figure S2-1. Other reconstructed protein NMR spectra. (a-1), (a-2) and (a-3) are spectra obtained with fully sampling, low-rank reconstruction, and VIP reconstruction for the 2D ^1H - ^{15}N HSQC spectrum of Ubiquitin; (b-1), (b-2) and (b-3) are spectra obtained with fully sampling, low-rank reconstruction, and VIP reconstruction for the 2D ^1H - ^{15}N best-TROSY spectrum of Ubiquitin. Note: 20% of fully sampled data were used in the reconstruction.

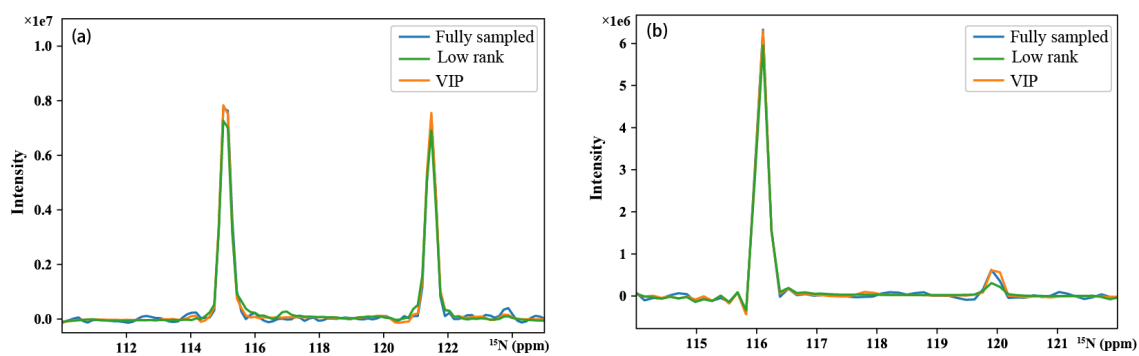


Figure S2-2. Zoomed out 1D ^{15}N traces. (a) and (b) are extracted from the location of dashed line marked in Figure S2-1. The blue, green and orange lines represent the spectra obtained with full sampling, low-rank and VIP methods, respectively.

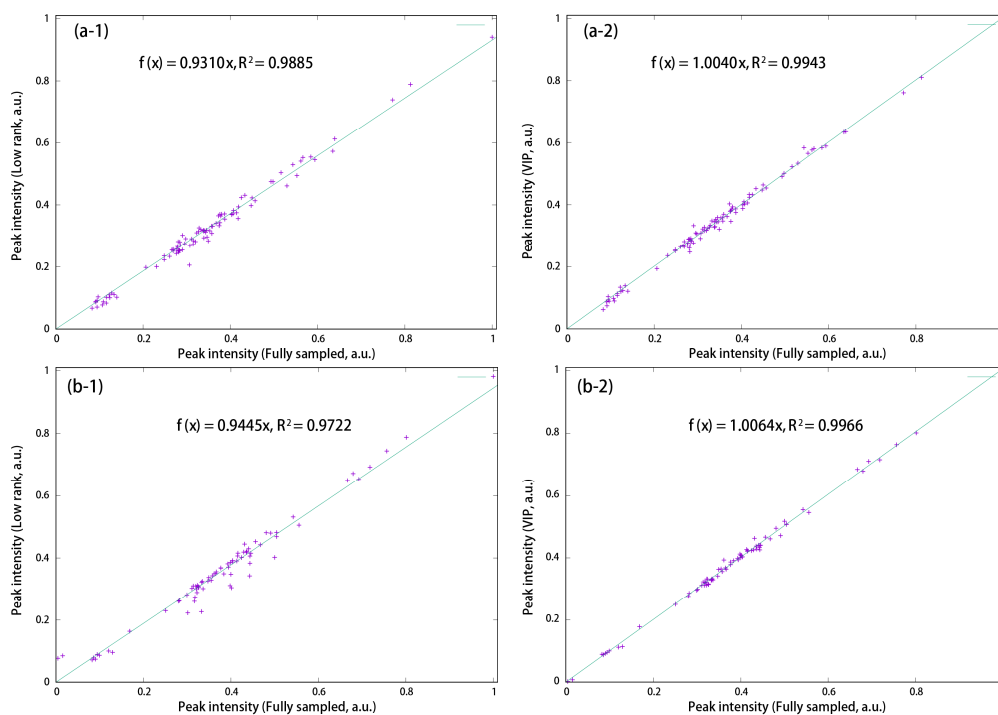


Figure S2-3. Intensity correlations for all peaks in protein NMR spectra. (a-1) and (a-2) are obtained by the low-rank and VIP methods on 2D ¹H-¹⁵N HSQC spectrum of Ubiquitin, respectively; (b-1) and (b-2) are obtained by the low-rank and VIP methods on 2D ¹H-¹⁵N best-TROSY spectrum of Ubiquitin, respectively. Note: The notation R^2 indicates the Pearson linear correlation coefficient of the fitted curve. The closer the value of R^2 gets to 1, the stronger the correlation between the reference and the reconstructed spectra is.

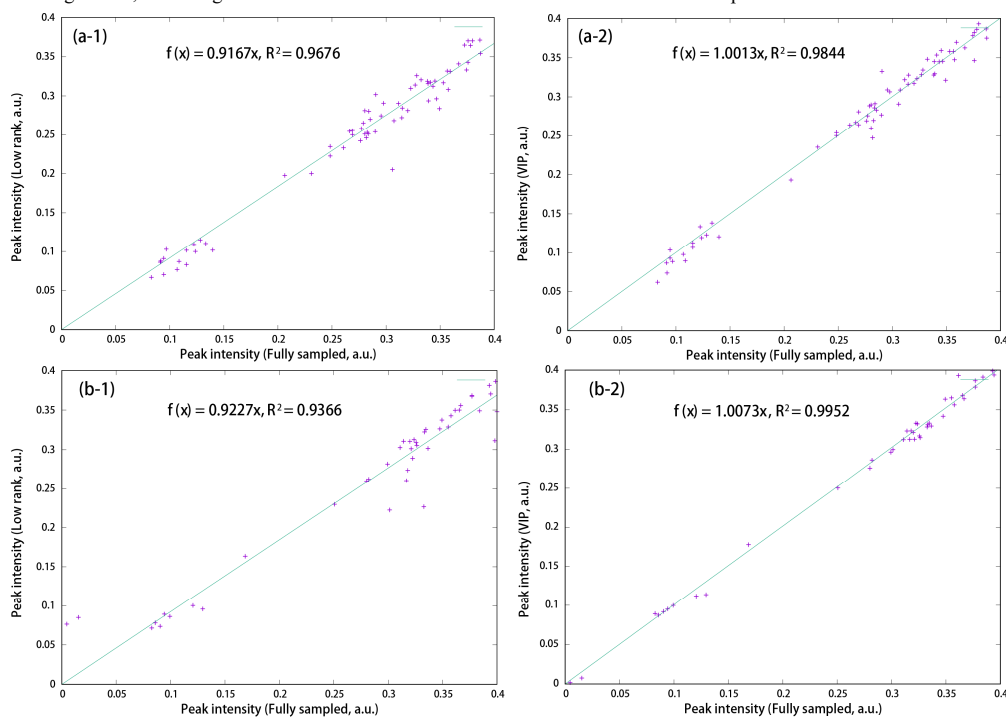


Figure S2-4. Intensity correlations for low-intensity peaks in protein NMR spectra. (a-1) and (a-2) are obtained by the low-rank and VIP methods on 2D ¹H-¹⁵N HSQC spectrum of Ubiquitin, respectively; (b-1) and (b-2) are obtained by the low-rank and VIP methods on 2D ¹H-¹⁵N best-TROSY spectrum of Ubiquitin, respectively.

S3. Measure internuclear distances from the NOESY spectra

The experiment of the 2D ^1H - ^1H NOESY spectrum of strychnine is reported in Supplement S7.

The peak correlation is shown as follow:

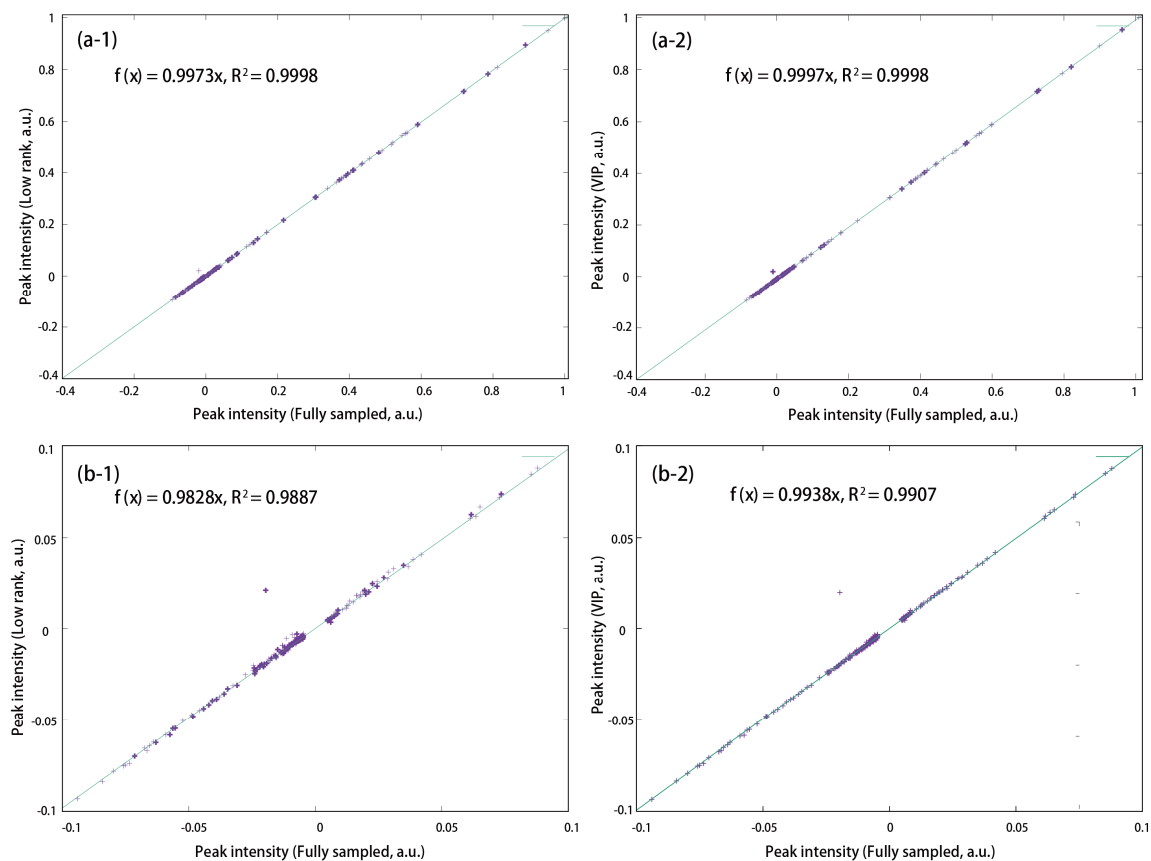


Figure S3-1. Correlations for all peaks and low-intensity peaks for the 2D ^1H - ^1H NOESY spectrum of strychnine. (a-1) and (a-2) are correlations obtained by the low-rank and VIP methods for all peaks, respectively. (b-1) and (b-2) are estimated with partial peaks of low intensities at a range of $[-0.1, 0.1]$ using the low-rank and VIP, respectively.

Table S3-1. The integral of the cross peak from NOESY spectra.

No. of points	Fully sampled spectrum	NUS reconstruction	
		Low-rank	VIP
H15a-H15b	1.00	1.00	1.00
H13-H15a	0.23	0.37	0.21
H14-H15a	0.08	0.20	0.07
H16-H15a	0.11	0.02	0.09
H15b-H16	0.13	0.29	0.11

Note: The integral value is normalized by dividing the maximal value (The integral value of the cross peak H15a-H15b).

S4. Measure the metabolic concentration of a mixture

The quantitative measure on the relative concentration is analyzed on a 2D ^1H - ^{13}C HSQC of a mixture of 3 metabolites, including D-Glucose, β -Alanine and Valine. The experiment is described in Supplement S7.

The 2D virtual HSQC₀ spectrum is obtained through a linear regression extrapolation by the HSQC_{*i*} (*i*=1,2,3)[1]:

$$\ln(A_{i,n}) = \ln(A_{0,n}) + i \times \ln(f_{A,n}), \quad i=1,2,3, \quad (\text{S4-1})$$

where $A_{i,n}$ is the peak volume, i.e. the integrated signal intensity, of the n^{th} peak in HSQC_{*i*}, and $A_{0,n}$ is the peak volume of the n^{th} peak in HSQC₀. The $A_{0,n}$ is free of attenuation during the coherence transfer period, and $f_{A,n}$ is the amplitude attenuation factor for the n^{th} peak [1]. Here, the peak integrals of an individual metabolic assignment in HSQC₀ is proportional to the metabolite concentration. Thus, the $A_{0,n}$ is chosen as the criteria to measure the concentration of metabolites. The peaks of assignment in a mixture of metabolic as shown:

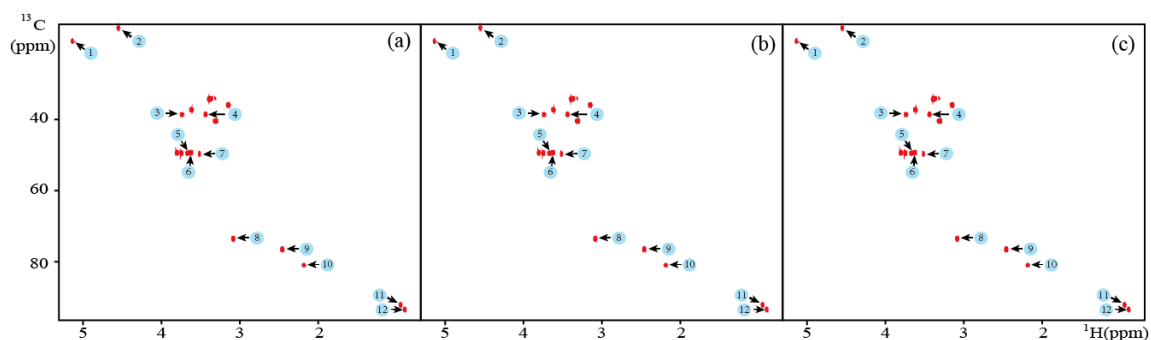


Figure S4-1. The 2D ^1H - ^{13}C HSQC_{*i*} (*i*=1,2,3) spectrum peak assignment (a)-(c) are the HSQC₁, HSQC₂ and HSQC₃, respectively. Note: 12 cross-peaks are labelled. Peaks 1-6 are assigned to Glucose, peaks 8 and 9 are assigned to Alanine, and peaks 7, 10, 11 and 12 are assigned to Valine.

We reconstructed the HSQC *i* (*i*=1,2,3) with 20% NUS data by the low rank and the VIP, respectively. The reconstruction result is shown in Figure S4-2. The first to third columns are the three HSQC_{*i*} (*i*=1,2,3) spectra of fully sampling, low-rank reconstruction, and VIP reconstruction, respectively.

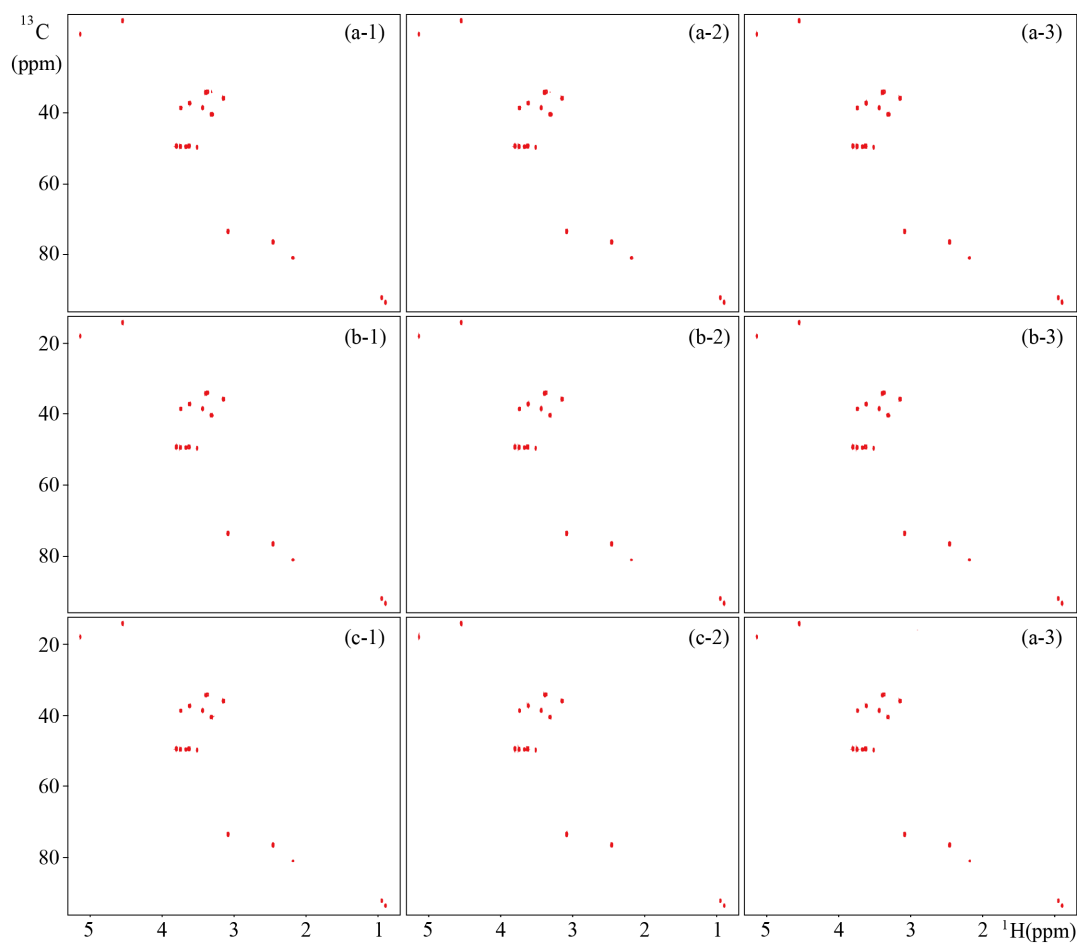


Figure S4-2. Reconstruction of 2D ^1H - ^{13}C HSQC_{*i*} (*i*=1,2,3) spectra of the HSQC. (a-1), (a-2) and (a-3) are spectra obtained with fully sampling, low-rank reconstruction, and VIP reconstruction for the 2D ^1H - ^{15}N HSQC₁ spectrum; (b-1), (b-2) and (b-3) are spectra obtained with fully sampling, low-rank reconstruction, and VIP reconstruction for the 2D ^1H - ^{15}N HSQC₂ spectrum; (c-1), (c-2) and (c-3) are spectra obtained with fully sampling, low-rank reconstruction, and VIP reconstruction for the 2D ^1H - ^{15}N HSQC₃ spectrum.

Twelve cross peaks are chosen to measure the relative concentration, which is calculated as the ratio of the volume of a metabolite over the volume of the Valine. Relative concentrations are estimated from spectra obtained with fully sampling, the low-rank and VIP reconstructions are reported in **Tables S4-1, S4-2, S4-3**.

Table S4-1. Extrapolated peak volumes (A_0) and measured peak volumes (A_1, A_2, A_3) from full sampled 2D HSQC $_i$ ($i = 1, 2, 3$) spectra.

Metabolites	Peak ID	Peak volumes						
		Measured on spectra			Extrapolated from HSQC $_i$ ($i=1,2,3$)			
		HSQC $_1$	HSQC $_2$	HSQC $_3$	HSQC $_0$	Average	Standard deviation	
Glucose	α	1	2.03×10^9	8.99×10^8	3.47×10^8	2.78×10^9	2.71×10^9	9.92×10^7
		3	2.03×10^9	9.72×10^8	3.93×10^8	2.76×10^9		
		4	1.91×10^9	9.43×10^8	4.40×10^8	2.56×10^9		
	β	5	2.02×10^9	9.99×10^8	4.54×10^8	2.72×10^9	4.33×10^9	5.40×10^7
		2	3.16×10^9	1.40×10^9	5.71×10^8	4.29×10^9		
	β -Alanine	6	3.27×10^9	1.89×10^9	9.27×10^8	4.37×10^9	3.64×10^9	2.32×10^8
8		5.18×10^9	2.66×10^9	1.26×10^9	3.48×10^9			
Valine	9	5.62×10^9	2.72×10^9	1.18×10^9	3.81×10^9	1.53×10^9	2.30×10^8	
	7	1.40×10^9	7.09×10^8	3.68×10^8	1.86×10^9			
	10	1.09×10^9	5.18×10^8	1.65×10^8	1.52×10^9			
	11	3.00×10^9	1.22×10^9	4.46×10^8	1.37×10^9			
	12	3.03×10^9	1.20×10^9	4.44×10^8	1.38×10^9			

Note: The peak volume, i.e. $A_{0,n}$, of the n^{th} peak in HSQC $_0$ is extrapolated from those volumes of the corresponding peak in HSQC $_1$, HSQC $_2$, HSQC $_3$ following the Eq.(S4-1). Peaks 1, 3, 4, 5 are assigned to D-Glucose (α) while peaks 2 and 6 are assigned to D-Glucose (β). The volume of D-Glucose is the sum of those of D-Glucose (α) and D-Glucose (β). The ratio D-Glucose: β -Alanine: Valine=7.04: 3.64: 1.53=4.60:2.38:1.

Table S4-2. Extrapolated peak volumes (A_0) and measured peak volumes (A_1, A_2, A_3) from reconstructed 2D HSQC $_i$ ($i = 1, 2, 3$) spectra using the low-rank approach.

Metabolites	Peak ID	Peak volumes						
		Measured on spectra			Extrapolated from HSQC $_i$ ($i=1,2,3$)			
		HSQC $_1$	HSQC $_2$	HSQC $_3$	HSQC $_0$	Average	Standard deviation	
Glucose	α	1	1.91×10^9	8.31×10^8	3.12×10^8	2.62×10^9	2.38×10^9	1.59×10^8
		3	1.72×10^9	8.33×10^8	3.63×10^8	2.33×10^9		
		4	1.71×10^9	8.82×10^8	3.88×10^8	2.31×10^9		
	β	5	1.68×10^9	8.53×10^8	3.83×10^8	2.27×10^9	4.21×10^9	2.92×10^7
		2	2.92×10^9	1.34×10^9	4.95×10^8	4.01×10^9		
	β -Alanine	6	3.30×10^9	1.62×10^9	7.86×10^8	4.42×10^9	3.46×10^9	1.89×10^8
8		4.96×10^9	2.56×10^9	1.22×10^9	3.33×10^9			
Valine	9	5.29×10^9	2.58×10^9	1.07×10^9	3.60×10^9	1.36×10^9	2.66×10^8	
	7	1.31×10^9	6.32×10^8	3.11×10^8	1.75×10^9			
	10	8.07×10^8	3.24×10^8	8.20×10^8	1.13×10^9			
	11	2.77×10^9	1.11×10^9	3.53×10^8	1.27×10^9			
	12	2.84×10^9	1.13×10^9	3.59×10^8	1.31×10^9			

Note: The ratio D-Glucose: β -Alanine: Valine= 6.59: 3.46: 1.36 =4.84:2.54:1

Table S4-3. Extrapolated peak volumes (A_0) and measured peak volumes (A_1, A_2, A_3) from reconstructed 2D HSQC $_i$ ($i = 1, 2, 3$) spectra using the VIP approach.

Metabolites	Peak ID	Peak volumes						
		Measured on spectra			Extrapolated from HSQC $_i$ ($i=1,2,3$)			
		HSQC $_1$	HSQC $_2$	HSQC $_3$	HSQC $_0$	Average	Standard deviation	
Glucose	α	1	2.01×10^9	8.96×10^8	3.54×10^8	2.74×10^9	2.65×10^9	1.05×10^8
		3	1.96×10^9	9.45×10^8	3.98×10^8	2.66×10^9		
		4	1.86×10^9	9.78×10^8	4.50×10^8	2.50×10^9		
		5	2.01×10^9	1.02×10^9	4.77×10^8	2.70×10^9		
	β	2	3.14×10^9	1.43×10^9	5.84×10^8	4.28×10^9	4.23×10^9	7.69×10^7
		6	3.19×10^9	1.61×10^9	9.29×10^8	4.17×10^9		
β -Alanine	8	5.17×10^9	2.62×10^9	1.26×10^9	3.46×10^9	3.61×10^9	2.11×10^8	
	9	5.55×10^9	2.67×10^9	1.15×10^9	3.76×10^9			
Valine	7	1.40×10^9	7.38×10^8	3.66×10^8	1.87×10^9	1.53×10^9	2.28×10^8	
	10	1.06×10^9	4.44×10^8	1.23×10^8	1.48×10^9			
	11	3.02×10^9	1.20×10^9	4.24×10^8	1.38×10^9			
	12	3.07×10^9	1.20×10^9	4.25×10^8	1.40×10^9			

Note: The ratio D-Glucose: β -Alanine: Valine= 6.88: 3.61: 1.53 =4.50:2.40:1

S5. Discussion on NUS rates

In this section, the reconstruction performance will be evaluated under different NUS rates, which are defined as the percentage of used measurements from the fully sampled data.

Results (Figure S5-1) indicate that the VIP significantly improves the correlation for all the tested data. Even under an extremely high acceleration factor (Figure S5-1(a)), e.g. the acceleration factor of 10 when the NUS rate is 10%, the VIP increases the correlation obtained with low-rank from 0.87 to 0.99. In addition, much lower standard deviations achieved by the VIP also indicates its more robustness to sampling trials.

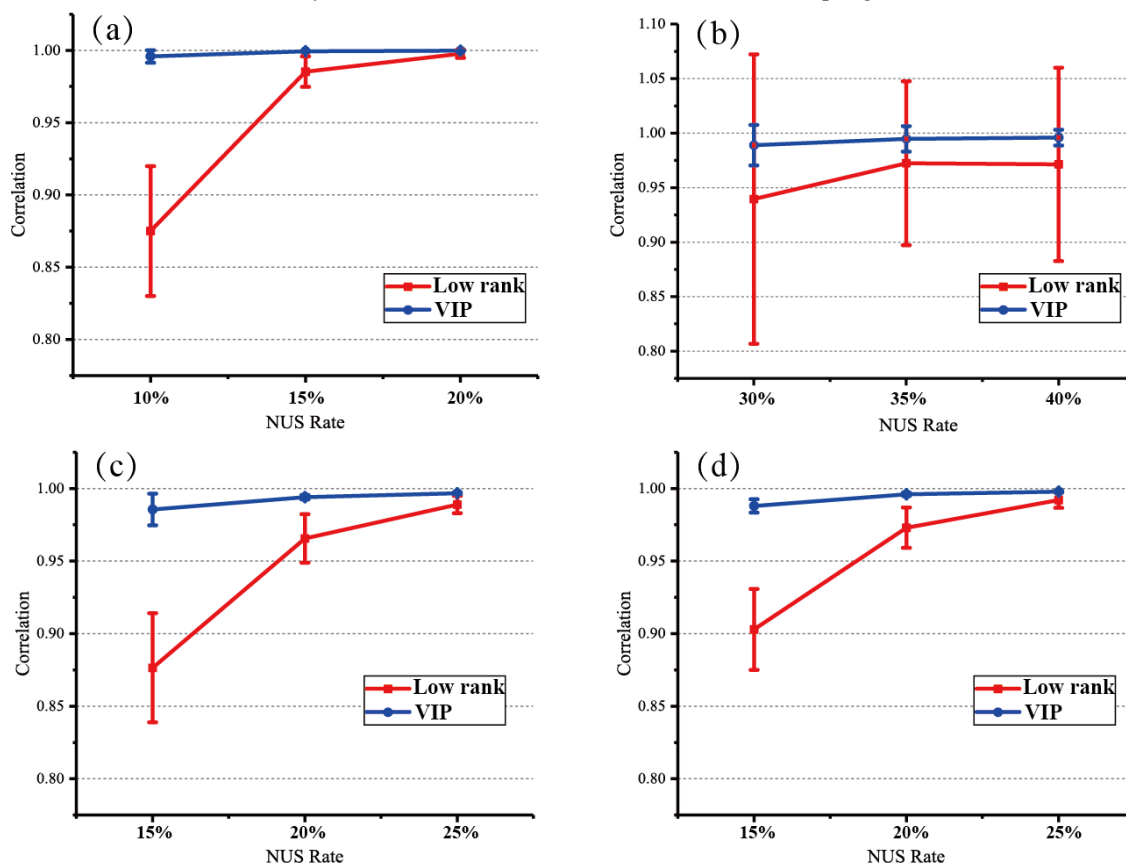


Figure S5-1. Peak intensity correlation for all tested real spectra under different NUS rates. (a)-(d) are for the HSQC of GB1, solid-state NMR magic-angle spinning spectrum, HSQC of Ubiquitin and TROSY of Ubiquitin, respectively. Note: The NUS rate is the percentage of used measurements from the fully sampled data. The error bars are the standard deviations of the correlations over 100 NUS sampling trials. The result is selected compressed sensing reconstruction spectrum as the initial reference.

S6. Discussion on the number of prior strong peaks

Detailed correlations are reported in Table S6-1.

Table S6-1. Peak intensity correlations versus the number of prior strong peaks (r)

Peak ID r	1	2	3	4	5
1	0.9088±0.1536	0.982±0.0359	0.9937±0.0092	0.9988±0.0022	0.9989±0.0008
2	0.9452±0.1188	0.9922±0.0109	0.9958±0.0055	0.999±0.0014	0.9991±0.0004
3	0.9799±0.0354	0.9948±0.0055	0.9982±0.0023	0.9994±0.0005	0.9992±0.0003
4	0.9901±0.0112	0.9972±0.0023	0.9988±0.0023	0.9995±0.0008	0.9992±0.0003
5	0.9864±0.0230	0.9979±0.0030	0.9991±0.0006	0.9996±0.0005	0.9993±0.0003
6	0.9698±0.0860	0.9961±0.0082	0.9984±0.0018	0.9995±0.0006	0.9992±0.0004
7	0.9673±0.0515	0.9944±0.0083	0.9981±0.0019	0.9995±0.0005	0.9992±0.0004
8	0.9243±0.1792	0.9770±0.1221	0.9956±0.0104	0.9993±0.0013	0.9990±0.0005
9	0.8864±0.2188	0.9587±0.1751	0.9939±0.0129	0.9988±0.0031	0.9989±0.0007
10	0.8028±0.2839	0.9388±0.2010	0.9826±0.0867	0.9981±0.0042	0.9986±0.0011
11	0.7702±0.2704	0.9323±0.1871	0.9866±0.0203	0.998±0.0033	0.9983±0.0012
12	0.6743±0.3259	0.9296±0.1248	0.9826±0.0256	0.9975±0.0035	0.9981±0.0013
13	0.5911±0.3605	0.8873±0.2016	0.9743±0.0327	0.9966±0.0047	0.9977±0.0018
14	0.5798±0.3472	0.8593±0.2155	0.9677±0.0447	0.9962±0.0044	0.9974±0.0020
15	0.5341±0.3476	0.8288±0.2435	0.9567±0.0650	0.9954±0.0053	0.9970±0.0023
16	0.4827±0.3473	0.7887±0.2702	0.9407±0.0956	0.9947±0.0070	0.9963±0.0028
17	0.4439±0.3519	0.7534±0.2979	0.9329±0.1008	0.9936±0.0085	0.9961±0.0028
18	0.4279±0.3553	0.7372±0.2885	0.9082±0.1484	0.9923±0.0123	0.9955±0.0033
19	0.4205±0.3513	0.7250±0.2825	0.9094±0.1329	0.9917±0.0143	0.9952±0.0035
20	0.3963±0.3522	0.6930±0.3163	0.8968±0.1283	0.9901±0.0155	0.9947±0.0037

Note: The numeric form $A \pm S$ where A is the mean of correlation and S is the standard deviation of correlations over 100 different NUS trials. For the compared low-rank method, the $A \pm S$ for peaks 1~5 are 0.8497±0.2107, 0.9685±0.0589, 0.9890±0.0201, 0.9981±0.0024, 0.9986±0.0009, respectively. The peaks 1~5 denote the peaks from the left to the right in Figure 2(a) of the main text. 8% of the fully sampled data is used in the NUS.

S7. Experimental setup

The Poisson-gap non-uniform sampling (NUS) [2] was used in all reconstructions.

2D ^1H - ^{15}N HSQC spectrum of GB1

The sample is 2 mM U- ^{15}N , 20%- ^{13}C GB1 in 25 mM PO_4 , pH 7.0 with 150 mM NaCl and 5% D_2O . Data was collected using a phase-cycle selected HSQC (hsqcfpf3gpwhg in Bruker library) at 298 K on a Bruker Avance 600 MHz spectrometer using a room temp HCN TXI probe, equipped with a z-axis gradient system. The fully sampled spectrum consists of 1146×170 complex points, the direct dimension (^1H) has 1146 data points while the indirect dimension (^{15}N) 170 data points.

2D ^1H - ^{15}N best-TROSY spectrum of Ubiquitin

The 2D ^1H - ^{15}N best-TROSY spectrum of ubiquitin was acquired at 298.2K temperature on an 800 MHz Bruker spectrometer and was described in previous paper^[3]. The fully sampled spectrum consists of 682×128 complex points, the direct dimension (^1H) has 682 data points while the indirect dimension (^{15}N) 128 data points.

2D ^1H - ^{15}N HSQC spectrum of Ubiquitin

The 2D ^1H - ^{15}N HSQC spectrum of Ubiquitin was acquired from ubiquitin sample at 298.2K temperature on an 800 MHz Bruker spectrometer and was described in previous paper^[3]. The fully sampled spectrum consists of 1024×98 complex points, the direct dimension (^1H) has 1024 data points while the indirect dimension (^{15}N) 98 data points.

2D ^1H - ^1H NOESY spectrum of strychnine

A NOESY spectra of 2.13 mg strychnine dissolved in 0.6 ml of CDCl_3 was acquired on a Bruker Avance III-HD 850 MHz spectrometer with a 5 mm CPTCI probe and collected using a phase sequence (noesygpwhg) at 298 K. Spectral widths were set to 8503.4 Hz in both proton dimensions, 28 scans per point with an inter-scan delay of 2 s and 400 ms mixing time. The fully sampled spectrum consists of 2048×256 complex points, the direct dimension (^1H) has 2048 data points while the indirect dimension (^1H) 256 data points.

2D ^1H - ^{13}C HSQC spectrum of the mixture (3 metabolites)

The sample is a mixture of 3 metabolites including 24.27 mM D-Glucose, 11.49 mM β -Alanine, 5.38 mM D-Mannose and dissolved in 0.5ml D_2O . Data was collected using a phase sequence (hsqcct2etgp2sq.2.khu) at 298 K on a Bruker Avance III-HD 850 MHz spectrometer using 5mm CPTCI probe. The fully sampled spectrum consists of 1024×256 complex points, the direct dimension (^1H) has 1024 data points while the indirect dimension (^{13}C) 256 data points.

References:

- [1] K. Hu, W. M. Westler, and J. L. Markley, "Simultaneous Quantification and Identification of Individual Chemicals in Metabolite Mixtures by Two-Dimensional Extrapolated Time-Zero ^1H - ^{13}C HSQC (HSQC_0)," *Journal of the American Chemical Society*, vol. 133, no. 6, pp. 1662-1665, 2011.
- [2] S. G. Hyberts, K. Takeuchi, and G. Wagner, "Poisson-gap sampling and forward maximum entropy reconstruction for enhancing the resolution and sensitivity of protein NMR data," *Journal of the American Chemical Society*, vol. 132, no. 7, pp. 2145-2147, 2010.
- [3] M. Mayzel, K. Kazimierczuk, and V. Y. Orekhov, "The causality principle in the reconstruction of sparse NMR spectra," *Chemical Communications*, vol. 50, no. 64, pp. 8947-8950, 2014.